Received: 7 October 2018 | Revised: 11 December 2018 | Accepted: 17 December 2018

DOI: 10.4218/etrij.2018-0554

SPECIAL ISSUE

WILEY ETRI Journal

Reducing speckle artifacts in digital holography through programmable filtration

Yongjun Lim[1] | **Jae-Hyeung Park**[2] | **Joonku Hahn**[3] | **Hayan Kim**[1] | **Keehoon Hong**[1] | **Jinwoong Kim**[1]

[1]Broadcasting and Media Research Laboratory, Electronics and Telecommunications Research Institute, Daejeon, Rep. of Korea.

[2]Department of Information and Communication Engineering, Inha University, Incheon, Rep. of Korea.

[3]School of Electronics Engineering, Kyungpook National University, Daegu, Rep. of Korea.

Correspondence
Yongjun Lim, Broadcasting and Media Research Laboratory, Electronics and Telecommunications Research Institute. Daejeon, Rep. of Korea.
Email: yongjun@etri.re.kr
and
Jae-Hyeung Park, Department of Information and Communication Engineering, Inha University, Incheon, Rep. of Korea.
Email: jh.park@inha.ac.kr

Funding Information
This research was supported by GigaKOREA project, (GK18D0100, Development of Telecommunications Terminal with Digital Holographic Table-top Display).

We propose a speckle reduction technique in electronic holographic display systems, where digital micro-mirror array devices are used as spatial light modulators. By adopting a programmable filtration in a general 4-*f* optic configuration, it is shown that the signal spectrum components in the frequency domain of a viewing-window-based holographic display system can be selectively filtered. Compared to the widely utilized single-sideband filtration techniques in electronic holographic display systems, our proposed programmable filtration can be utilized to effectively reduce the speckles in the reconstruction of point-cloud-based computer-generated holograms. Experimental results are presented to verify our proposed concept.

KEYWORDS
holographic display, holography, spatial filter, speckle, speckle reduction

1 | INTRODUCTION

Speckle is one of the most intrinsic properties of digital holographic display systems exhibited when coherent light sources such as lasers are applied in the play back process of computer-generated holograms (CGHs) [1–3]. Highly correlated wave fields of coherent light sources make unwanted granular patterns, that is, speckle artifacts appear in general electronic holographic display systems, which degrade the image quality of the reconstructed holograms. To reduce or remove speckle patterns, various methods have been proposed. In fundamental approach, incoherent or partially coherent light sources are utilized [4,5]. However, the low power throughput and broad linewidth of the light sources result in a relatively weak intensity and blurring of the reconstructed three-dimensional holographic scenes. Recently, novel works have been proposed for solving speckle artifacts in capturing objects with digital

holographic schemes. They can be classified into two categories, that is, numerical approaches and optical techniques [6]. Numerical approaches fundamentally refer to image processing techniques and statistical analysis, and these schemes have shown good performance in holographic image denoising [6]. Uzan et al. showed that a nonlocal means (NLM) filtering method can be applied to speckle noise reduction in digital holography [7]. Bianco et al. adopted an enhanced grouping algorithm and a sparsity enhancement filtering scheme, using which they could remove the noise factors including speckle artifacts [8]. Leo et al. proposed a technique utilizing the pixel location of temporally sequential images to suppress speckle patterns [9,10]. Memmolo et al. provided an encoding technique based on a combination of multiple holograms, and they proved that it could improve the image quality in optically reconstructed holograms [11]. Rivenson et al. applied a compressive sensing scheme in an incoherent holographic display system and showed that effective depth range as well as good image quality could be achieved [12]. In contrast, methods for reducing speckles from a given three-dimensional (3D) object dataset have been reported lately. A spatial interleaving technique that sequentially displays spatially interleaved subsets of a 3D scene was reported [13,14]. This technique, however, is limited only to point-cloud-based CGHs, being not applicable to general CGHs. Recently, an angular spectrum interleaving technique for mesh-based CGHs as well as for point-cloud-based CGHs was proposed [15]. The main concept is to deliver only the spectral components associated with a single plane carrier wave to the user's eye at a time. Consequently, there is no interference between the different spectral component sets associated with different plane carrier waves, and thus, the speckle artifacts can be effectively reduced. The depth of the field broadening caused by presenting the spectral components associated with only a single plane carrier wave is reduced by presenting the spectral components associated with different plane carrier waves sequentially in a time-multiplexing manner.

In the implementation of digital holographic displays with time-multiplexing, digital micro-mirror array devices (DMDs) are usually used for their fast refresh rate. Because a DMD has a limited modulation property, that is, only binary amplitude modulation [16–18], single-sideband (SSB) filtering is generally applied to allow an appropriate hologram spectrum in the frequency domain to pass through [19,20] while blocking the unwanted spectrum caused by the binary modulation. Nevertheless, previously reported work on speckle reduction using angular spectrum interleaving [15] did not clarify the effective region for filtration in a digital holographic display system where DMDs are used to display binary-type holograms.

In this paper, we show that the binarization of the amplitude holograms in the numerical process of CGHs can induce unwanted spectral components in the frequency domain or in a spatial filter position. In case of utilizing a single plane carrier wave technique, it is shown that the effective spectral zone in the filter domain should be much smaller than the maximum size allowed for usual SSB holography to block the unwanted spectral components caused by the binary modulation. To solve this problem, we propose a programmable dynamic filtration method to reduce the speckle artifacts using the angular spectrum interleaving technique in digital holographic display systems where a DMD is used as a spatial light modulator (SLM). To achieve dynamic filtration in the spectrum domain, another DMD is used in the Fourier plane of a 4-*f* optics. Therefore, in our proposed method, two DMDs are used, that is, one as an SLM and the other as a programmable filter. In the experiment, we measure the speckle contrast values in the conventional and proposed systems for quantitative comparison.

2 | FUNDAMENTAL CONCEPTS

In this section, we briefly describe a single-carrier-wave technique for reducing the speckle distribution in point-cloud-based CGHs of viewing-window-based holograms. Considering the use of DMDs as SLMs, a general filtering method adopting an SSB in the reconstruction of amplitude-type holograms and the unwanted signals given by their binarization are described. After describing the binarization of amplitude-type holograms, the unwanted signal intervention in the SSB is provided.

2.1 | Angular spectrum interleaving technique for reducing speckle artifacts in point-cloud-based CGHs

The fundamental concept of the angular spectrum interleaving technique reported in [15] was to deliver the angular spectrum associated with only a single plane carrier wave to the user's eye at a time. In [15], it was demonstrated with mesh-based CGHs using a simple holographic display setup. This technique can be readily modified to be applied to point-cloud-based CGHs for viewing window-type holographic displays. In the viewing window-type holographic displays, a point-cloud-based CGH is synthesized by [21]

$$U(x,y) = \sum_m a_m \exp(j\theta_m) \frac{\exp\left[j\frac{2\pi}{\lambda} r_m\right]}{r_m}, \tag{1}$$

where a_m and θ_m are the amplitude and phase, respectively, of the object point located at (x_m, y_m, z_m), and λ is the wavelength. r_m in (1) is given by

$$r_m = \sqrt{(x_{mi} - x)^2 + (y_{mi} - y)^2 + z_{mi}^2}, \quad (2)$$

where (x_{mi}, y_{mi}, z_{mi}) is related to the displayed object point location (x_m, y_m, z_m) in the viewing window-type holographic display using a converging lens of focal length f by

$$z_{mi} = \frac{fz_m}{f - z_m},\ x_{mi} = \frac{fx_m}{f - z_m},\ y_{mi} = \frac{fy_m}{f - z_m}. \quad (3)$$

In usual point-cloud-based CGHs, phase θ_m of the object point is given by a random value. In the angular spectrum interleaving technique, however, phase θ_m of the object point is given for a plane carrier wave having spatial frequency pair (ν_{xo}, ν_{yo}) by

$$\theta_m = 2\pi\left(\nu_{xo}x_{mi} + \nu_{yo}y_{mi} + z_{mi}\sqrt{\frac{1}{\lambda^2} - \nu_{xo}^2 - \nu_{yo}^2}\right). \quad (4)$$

Equation (4) structures the phase distribution on the displayed 3D object surfaces according to the single plane carrier wave of spatial frequency pair (ν_{xo}, ν_{yo}). Therefore, in the Fourier plane of the hologram, the spectrum of hologram $U(x, y)$ is centered around plane carrier wave spatial frequency pair (ν_{xo}, ν_{yo}) with a width given by the bandwidth of the 3D object itself. Because the spectrum is associated only with a single plane carrier wave, there is no interference between the different plane carrier wave components, and thus, the speckle artifact is removed at the expense of the enlarged depth of field of the reconstruction. In the angular spectrum interleaving technique, multiple holograms are synthesized with different spatial frequency pairs of the plane carrier waves. Moreover, they are presented sequentially, such that the temporal accumulation of the spectrum fills the entire spectral area supported by the pixel pitch of the SLM, giving speckle-free and narrow-depth-of-field 3D holographic images.

2.2 | Multiple spectral components caused by binary amplitude modulation of DMD

As described in section 2.1, for a speckle-free reconstruction using the angular spectrum interleaving technique, the spectral components associated only with a single plane carrier wave should exist in each frame of the time-multiplexing. However, the amplitude binary modulation property of the DMD generates multiple harmonics in each frame, dissatisfying this requirement. Let us denote the amplitude and phase of ideal complex field hologram $U(x, y)$ in (1) as $A(x, y)$ and $\phi(x, y)$, respectively, such that $U(x, y) = A(x, y)\exp[j\phi(x, y)]$. Ideal complex field $U(x, y)$ is encoded into a real-valued pattern by adding its complex conjugate based on the SSB encoding technique, and then it is binarized by

$$\begin{aligned} b(x,y) &= B[U(x,y) + U^*(x,y)] \\ &= B[2A(x,y)\cos\phi(x,y)] \\ &= \begin{cases} 1, & if\ \cos\phi(x,y) > 0 \\ 0, & \text{otherwise} \end{cases}, \end{aligned} \quad (5)$$

where $B[\cdot]$ represents a binarization operator. This binary pattern, $b(x, y)$, is loaded to the DMD.The multiple harmonics in the spectrum of binary pattern $b(x, y)$ is readily understood by expanding it using a Fourier series with respect to phase $\phi(x, y)$. From the last line of (5), it is evident that $b(x, y)$ is a periodic function of $\phi(x, y)$ with fundamental period 2π. Then $b(x, y)$ can be written as

$$b(x,y) = \sum_{n=-\infty}^{\infty} C_n \exp[jn\phi(x,y)], \quad (6)$$

with Fourier coefficient C_n given by

$$C_n = \frac{1}{2\pi}\int_{-\pi}^{\pi} b(\phi)\exp[-jn\phi]d\phi = \frac{1}{2\pi}\int_{-\pi/2}^{\pi/2}\exp[-jn\phi]d\phi, \quad (7)$$

where $b(x, y)$ is denoted by $b(\phi)$ to stress that it depends on ϕ by (5). After some manipulations, (6) and (7) reduce to

$$b(x,y) = \frac{1}{2} + \frac{2}{\pi}\sum_{n=1}^{\infty}\frac{(-1)^{n+1}}{2n-1}\left\{e^{j(2n-1)\phi(x,y)} + e^{-j(2n-1)\phi(x,y)}\right\}. \quad (8)$$

Equation (8) indicates that binarized pattern $b(x, y)$ contains not only the desired term, that is, $\exp[j\phi(x, y)]$, but also direct current (DC) term 1/2, conjugate $\exp[-j\phi(x, y)]$, and many other harmonics $\exp[\pm j(2n - 1)\phi(x, y)]$ (where $n = 2, 3, 4, \ldots$). Therefore, even though ideal complex field hologram $U(x, y)$ is synthesized with a single plane carrier wave such that its spectrum is concentrated around single carrier wave spatial frequency pair (ν_{xo}, ν_{yo}), binarized amplitude pattern $b(x, y)$ has multiple spectral components centered at $((2n - 1)\nu_{xo}, (2n - 1)\nu_{yo})$ (where $n = \pm1, \pm2, \pm3, \ldots$) and (0, 0). With a viewing window-type holographic display with a 4-f optics filter plane of focal length f_1 as shown in Figure 1A, the spectra of ideal complex field $U(x, y)$ and binarized pattern $b(x, y)$ for a single plane carrier wave are illustrated in Figures 1B, C, respectively. Here, the pixel pitch of the DMD is denoted by p. As shown in Figure 1C, inside the usual filtration area (i.e., aperture area) of the SSB technique, the binary modulation generates multiple harmonics, which interfere with each other in the reconstruction, generating speckle artifacts even in the single plane carrier wave case.

3 | PROPOSED METHOD

3.1 | Working principles

As is described in the previous section, an unwanted spectrum is generated in the process of binary modulation, and

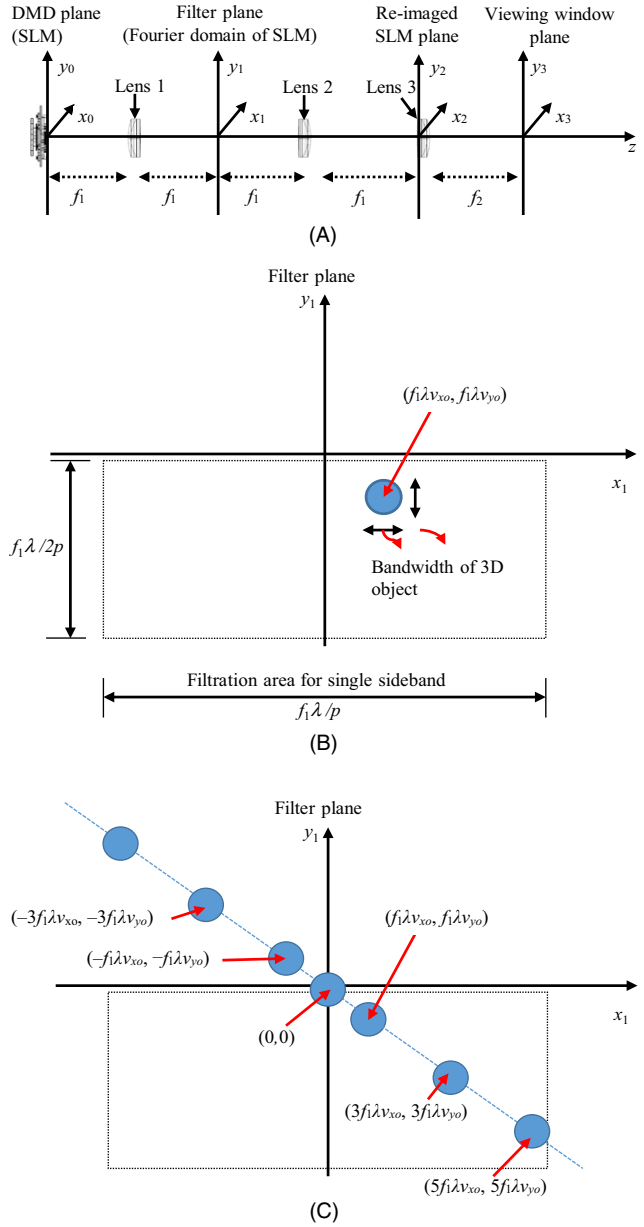

FIGURE 1 (A) is the fundamental configuration for electronic display systems adopting viewing window and 4-*f* optics, (B) shows the spectrum of ideal complex field $U(x, y)$ associated with a single plane carrier wave of spatial frequency pair (ν_{xo}, ν_{yo}) in the filter plane of the 4-*f* optics, and (C) shows the spectrum of binarized amplitude pattern $b(x, y)$ in the same plane

this can be added in the filtering zone of conventional SSB. As a consequence, a single carrier wave spectrum can be affected by the intrusion of unwanted signal components, and so, the speckle artifacts can be increased than expected. Here, we describe a novel filtration scheme to reduce speckle artifacts in an effective way. The fundamental concept for our novel filtration technique is presented in Figure 2.

As is presented in Figure 2, the filter size of the conventional SSB is larger than that of the single carrier wave sets when the speckle artifacts are required to be reduced.

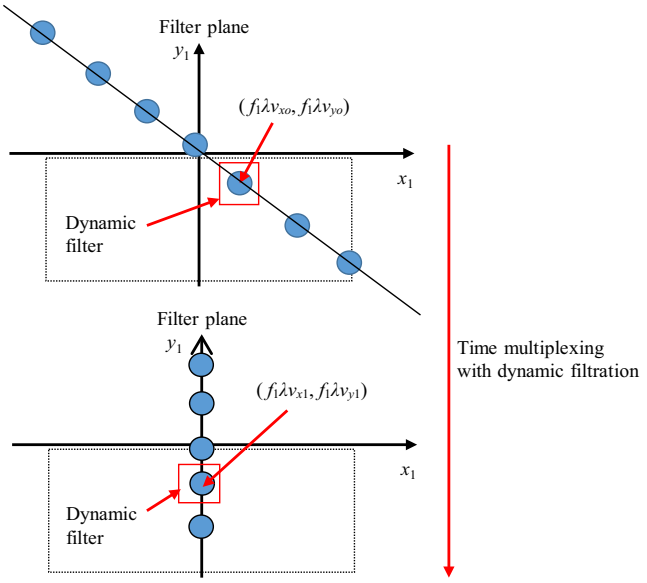

FIGURE 2 The proposed method for excluding false components and for enabling programmable filtration is described

In addition, mixing of the different spectral components of the single carrier wave sets or enabling temporal multiplexing of several spectral components simultaneously needs to be achieved. Therefore, it is desirable to implement passing through the necessary region dynamically and synchronize the filter region with which the CGH images are displayed on the SLM DMD. As is described in a previous work, it is enough to mix four holograms with different carrier wave sets to provide wide viewing angles and narrow depths of fields [15]. As a consequence, an effective method for filtering signal components is required for the speckle reduction techniques adopting single carrier wave sets. In other words, the first order in (8) should be filtered in accordance with the CGH displayed on the SLM DMD, and four other different sets should be temporally multiplexed simultaneously. To achieve those concepts, it is necessary to use a dynamically controllable device, and we place another DMD in the filter position.

3.2 | Implementation of a programmable filter

To implement a programmable filtration technique, we use another DMD as a dynamic filter or a programmable filter. In particular, in Figure 3, DMD 1 is used to display the point-cloud-based CGHs, whereas DMD 2 is placed at the back focal plane of lens 1 and applied to reflect a proper signal spectrum according to DMD 1. Lens 2 is the second lens in the 4-*f* optics configuration, and lens 3 is a field lens in the viewing-window-based holographic display system [22,23]. A charge coupled device (CCD) captures the reconstructed holograms, and the captured images are utilized to estimate the speckle patterns.

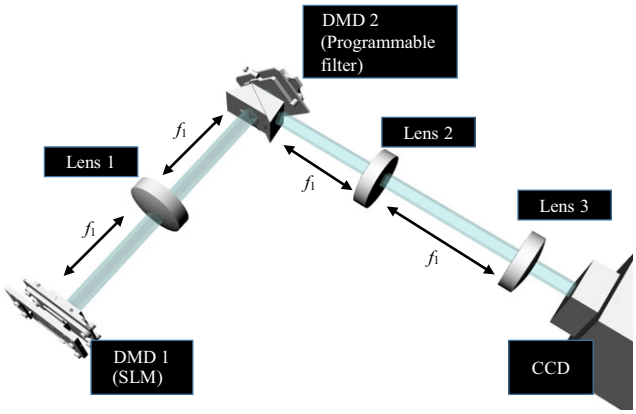

FIGURE 3 The scheme for the proposed filtration method in viewing-window-based holographic display systems

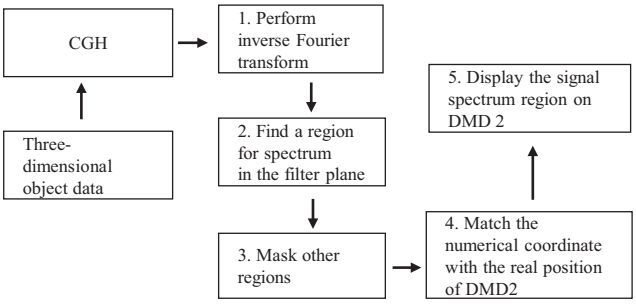

FIGURE 4 Shows the flowchart for generating a filtering region on the DMD used as a programmable filter

To use a DMD as a programmable dynamic filter, we describe the procedure for launching the filtering region on the filter DMD, as is presented in Figure 4. CGHs are generally given by the 3D object data, and the inverse Fourier transform of the CGHs can generate the spectral components at the filter plane in the first step. Then, the signal spectrum region for the holograms can be found numerically in the second step, and the masking of other regions, except for the signal spectrum, occurs in the third step. As the coordinate in the numerical process does not match the real coordinate of filter DMD 2, coordinate transformation should be performed in the last step. Finally, the images for the filter region are displayed on DMD 2.

4 | EXPERIMENTAL VERIFICATION

4.1 | Experimental set-up and preparation

In Figure 5A, the schematic of the experimental set-up is presented, and its image is shown in Figure 5B.

In the experimental set-up, a 532 nm laser (Samba™, Cobolt Corp.), the maximum optical power of which is 100 mW, is used as a coherent light source, and two DMDs having 1,024 (horizontal) × 768 (vertical) pixels

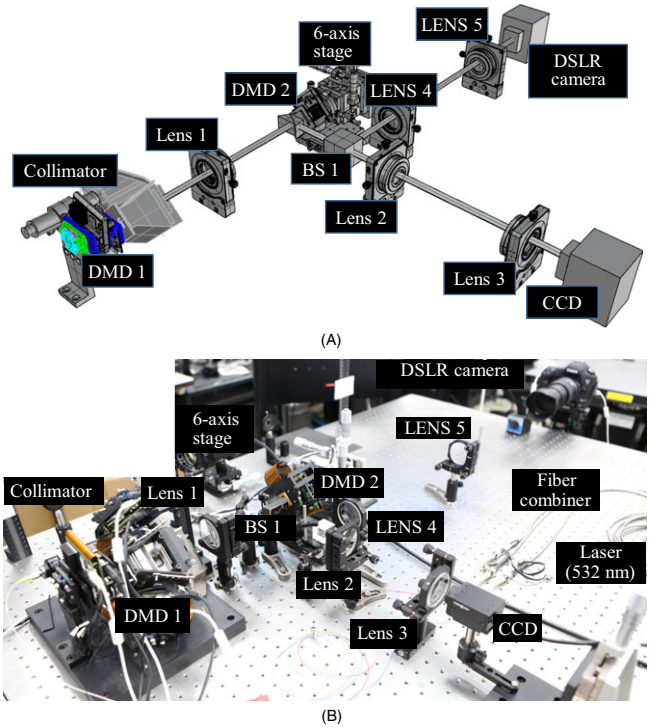

FIGURE 5 (A) is the schematic of the experimental set-up, and (B) is the corresponding real picture

are applied. One is used as an SLM to display the binary-type CGHs, and the other is used as a programmable filter. The pixel size of both the DMDs is 13.68 μm, and the maximum operating speed is approximately 22 kHz (V-7000, Vialux GmbH). The focal length of lens 1 and lens 2 is 150 mm, whereas that of lens 4 and lens 5 is 180 mm. To illuminate DMD 1, which is used as the SLM, a collimator and transmission-type total internal reflection (TIR) prism are placed in front of it, whereas a reflection-type TIR is placed in front of DMD 2, used as the programmable dynamic filter. The specific description of the two different TIR prisms for illuminating DMDs can be found in [24,25]. Lens 1 is a Fourier lens, and it converts the optical field emanating from DMD 1 into spatial frequency components, and DMD 2 is placed in the Fourier plane generated by lens 1 and DMD 1. DMD 2 is launched at a six-axis stage, with three axes for translation and three axes for roll, pitch, and yaw, to align DMD 2 as fine as possible. One beam splitter, denoted by BS 1 in Figure 5, separates the beam path into two paths. One passes through lens 2 and lens 3, and it reaches the CCD, and the other passes through lens 4 and lens 5. The CCD (Grasshopper 3, Point Grey Corp.) has a pixel number of 4,240 (horizontal) × 2,848 (vertical) and pixel pitch of 3.45 μm, and it captures images of the reconstructed holograms. In capturing the hologram images, no lens is placed in front of the CCD, that is, objective measurement for speckle is applied. Lens 4 and lens 5, constituting another

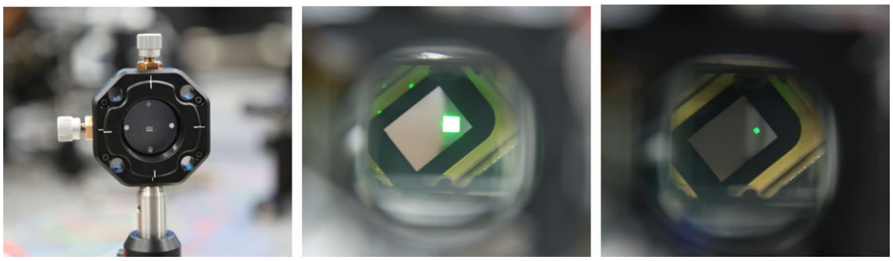

FIGURE 6 (A) is the image of a conventional SSB filter, the center of which is applied as the filtering area. (B) is the captured image of a programmed SSB filter on DMD 2, and (C) is the captured image of a programmed filter image for a single carrier wave technique on DMD 2

4-*f* optics, are inserted to ensure DMD 2 identifies the filter position conveniently. The captured images of the filter plane, DMD 2, by a DSLR camera (5D MARK III, Canon Corp.) are presented in Figures 6B, C. Figure 6A shows the conventional SSB filter, where half the region of the SSB is implemented for the experiment. The implemented SSB filter on DMD 2 is shown in Figure 6B, and the implemented region for the single carrier wave technique on DMD 2 is shown in Figure 6C. In Figures 6A, B, the size of the filter region for the SSB is given by $(f_1\lambda/2p) \times (f_1\lambda/2p)$, where $f_1 = 150$ mm, $\lambda = 532$ nm, and $p = 13.68$ μm. The corresponding pixel numbers displayed on DMD 2 are 214 × 214. In the experiment for the programmable filtration, the actual position is changed according to the single carrier wave sets. Consequently, the filter region shown in Figure 6C can be varied and synchronized with the image displayed on the SLM DMD. The filter region shown in Figure 6C is given by following the process presented in Figure 4, and the estimated pixel numbers are 70 (horizontal) × 70 (vertical).

To verify the effectiveness of the proposed programmable filter in terms of the speckle artifact reduction, the speckle contrast value is used to quantify the measured speckles [26,27]. The speckle contrast is given by

$$\mathrm{SC} = \frac{\sigma}{\langle I \rangle}, \tag{9}$$

where $\langle I \rangle$ and σ represent mean values of the intensity and standard deviation of the captured images, respectively. We design the test pattern for measuring the speckle distribution, and the test image pattern referring to the conventional USAF 1951 is shown in Figure 7, the center of which is composed of the rectangular region for the calculation of speckle contrast values. The entire size of the test image is 1,024 × 768 pixels and that of the square at the center is 150 × 150 pixels.

In Figure 8, the CGH images of the four different sets given by the single carrier wave technique for point-cloud-based holograms are presented. Figures 8A, C, E, and G are the CGHs of the four different single carrier wave sets, and they are to be displayed on DMD 1 (SLM). The

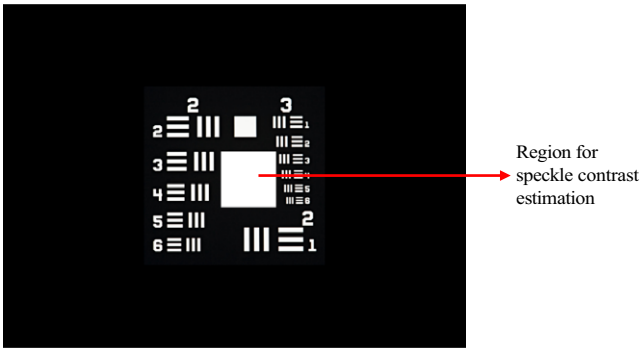

FIGURE 7 The test pattern for speckle estimation is described

corresponding filter images given by referring to the procedure presented in Figure 4 are, respectively, shown in Figures 8B, D, F, and H, and these are to be uploaded on DMD 2 (programmable filter).

In Figures 8B, D, F, and H, the positions on the DMDs are 40 pixels away from one another horizontally and vertically because they have different carrier wave sets.

4.2 | Experimental results

In this subsection, experimental results to verify the proposed concept are presented. First, we conduct three types of experiments depending on the filtering condition. One is based on the conventional method, which implies that the conventional SSB is placed in the filter plane and adopts the SSB filter shown in Figure 6A. Another is to adopt SSB on DMD 2, as shown in Figure 6B, the case of which is to include the false spectral components in the SSB region while using DMD 2 in the filter plane. In these two experiments, half of the SSB along the horizontal direction is applied. The other experiment is the programmable filter test on DMD 2, as presented in Figure 6C, which is the main experiment for our proposed concept. Results for these three types of experiments are displayed in Figure 9. To compare the results easily, they are listed and grouped in three columns. Four images, Figures 9A, D, G, and J in the left column of Figure 9 denoted by conventional SSB show the reconstructed holograms of the conventional SSB

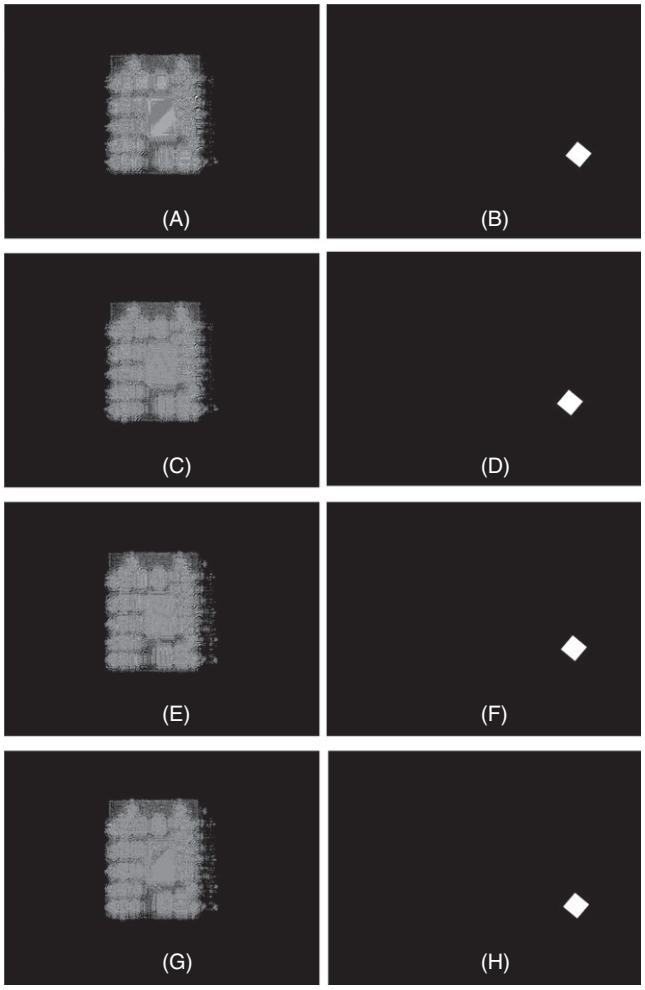

FIGURE 8 (A), (C), (E), and (G) are the CGHs of the test patterns of the four different sets of the single carrier wave technique, which are to be uploaded on DMD 1 (SLM). (B), (D), (F), and (H) are the corresponding images for the programmed filter region to be displayed on DMD 2

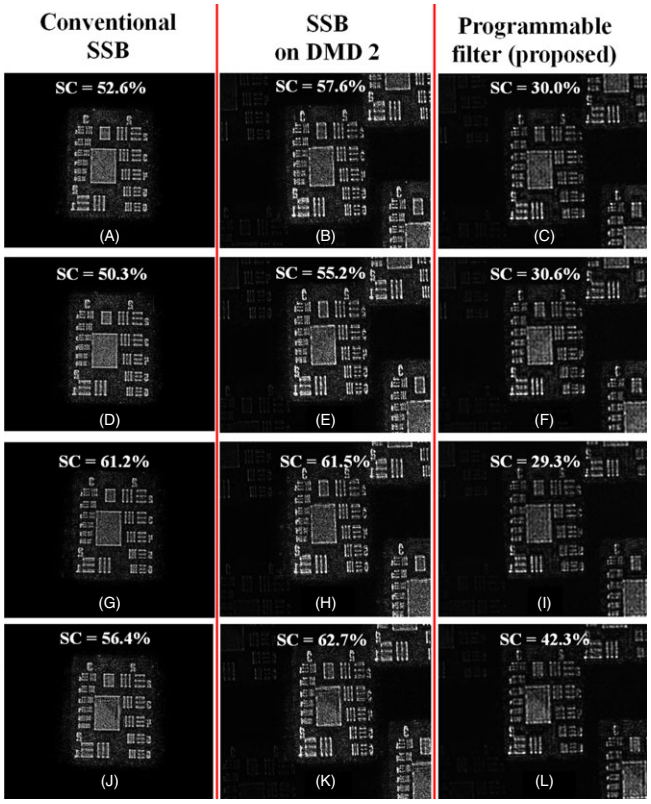

FIGURE 9 (A), (B), and (C) are the reconstructed hologram images of the CGH in Fig. 8(A). (D), (E), and (F) are the reconstructed hologram images of the CGH in Figure 8(C). (G), (H), and (I) are the reconstructed hologram images of the CGH in Figure 8(E). (J), (K), and (L) are the reconstructed hologram images of the CGH in Figure 8(G)

experiments. Four images, Figures 9B, E, H, and K in the middle column of Figure 9 denoted by SSB on DMD 2 present the results for the SSB filter on DMD 2. Four images, Figures 9C, F, I, and l in the right column of Figure 9 denoted by programmable filter present the experimental results for the proposed concept.

In Figure 9, the estimated speckle contrast values are inserted in the upper region of each image. The captured images in the experiments are horizontally flipped because of the reflection-type TIR prism for illuminating DMD 2.

Second, the temporal multiplexing experiments for four different carrier wave CGHs were performed, where the results were given by temporally multiplexing the CGHs shown in Figures 8A, C, E, and G. For the conventional SSB experiment, only DMD 1 is activated, where the filter presented in Figure 6A is used.

The captured hologram image for the conventional SSB experiment is shown in Figure 10A. The estimated speckle distribution for the inset square region is presented in Figure 10B, and its speckle contrast value is 34.7%. The experimental result with the SSB on DMD 2 is presented in Figure 10C. The corresponding speckle contrast value is 30.5%, the speckle distribution of which is presented in Figure 10D. The result for the programmable filter experiment is presented in Figure 10E. The speckle contrast value is 20.2%, and the speckle distribution is shown in Figure 10F. In these temporal-multiplexing experiments, the repetition rate of both the DMDs is set as 3,600 Hz, and they are synchronized for the programmable filter experiments. In synchronizing and displaying the CGHs on DMD 1 and DMD 2, commercial software LabVIEW was applied.

Regarding the resolution confirmation of the proposed method, we perform an additional experiment. In Figures 11A, B, the third group in the USAF image is enlarged and shown in the left side of the corresponding holograms. In both the magnified images, horizontal and vertical bars less than the third element in the third group become indistinguishable. Thus, by comparing the resolution image of the program filter with that of the SSB filter

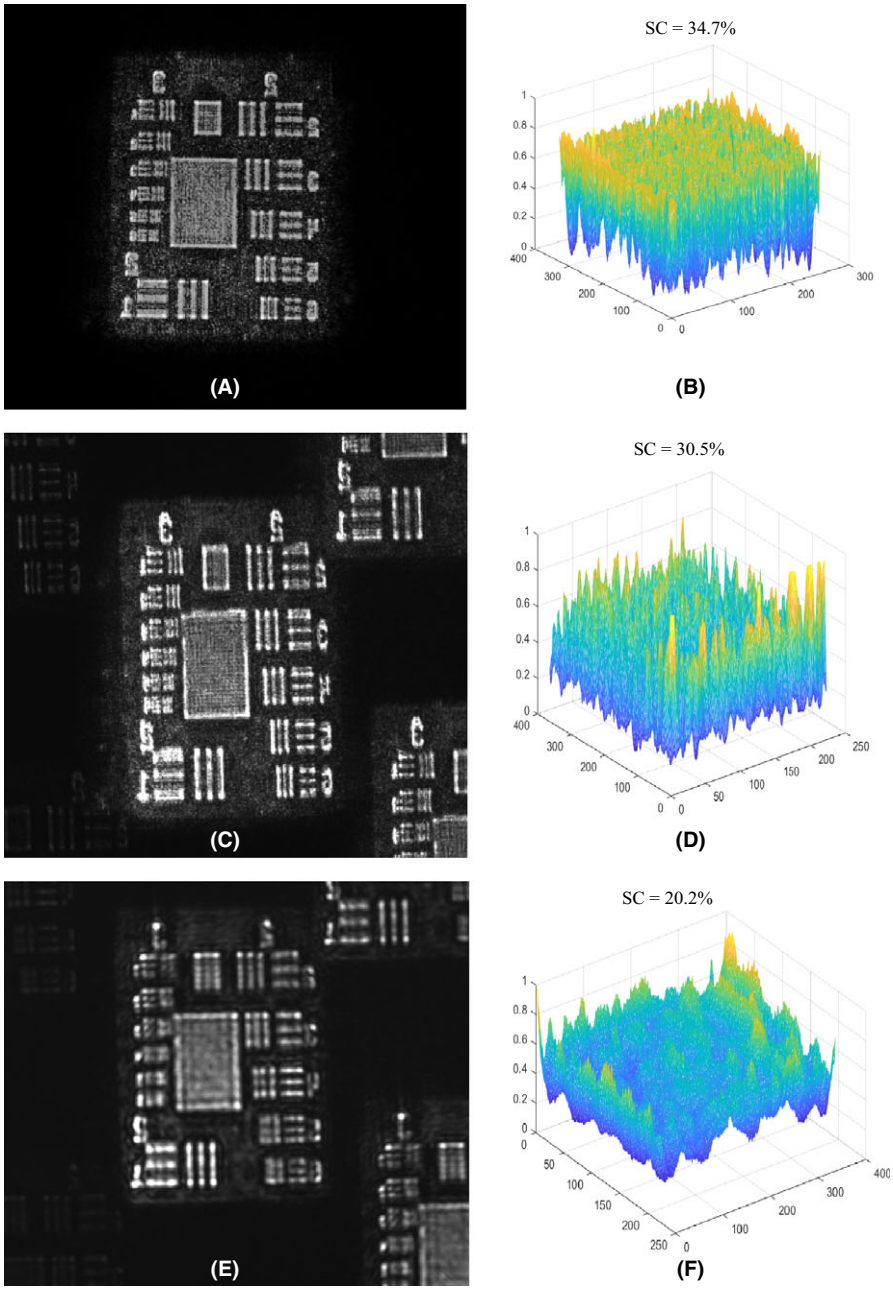

FIGURE 10 (A), (C), and (E) are the temporally multiplexed results for the four different single carrier wave sets presented in Figure 8 (A), (C), (E), and (G). Their corresponding speckle distributions are, respectively, shown in (B), (D), and (F) with the calculated speckle contrast values

on DMD 2, it is observed that the use of the programmed filter does not cause resolution to be lowered.

5 | DISCUSSION

As is seen from the experimental results in Figures 9 and 10, the programmable filter achieved by the use of a DMD effectively reduces the speckle artifacts. The speckle contrast values for the programmable filter case are smaller than those for the conventional SSB methods, as shown in Figure 9. In the temporal multiplexing experiments, the speckle contrast value for the programmable filter is the lowest of all the experiments. Another characteristic approach is to synchronize the SLM DMD with the programmable filter DMD dynamically, which has not been shown in previous works regarding speckle reduction techniques as well as filtering methods for binary-type holograms. This feature would be particularly useful if our proposed method was to be applied in other holographic research such as synthetic aperture holograms, where dynamic filters can be applied. However, owing to the relatively small pixel pitch of DMD 2 compared to that of the spectrum region of the single carrier wave holograms, replicas of hologram signals are observed in Figures 9 and 10, where DMD 2 is implemented as a programmable dynamic filter. This is caused by the periodic pixel pitch of DMD 2 placed in the filter plane. To remove this, the pixel size should be increased to the size of the signal spectrum. Although we used a DMD as a filter, fast-activating

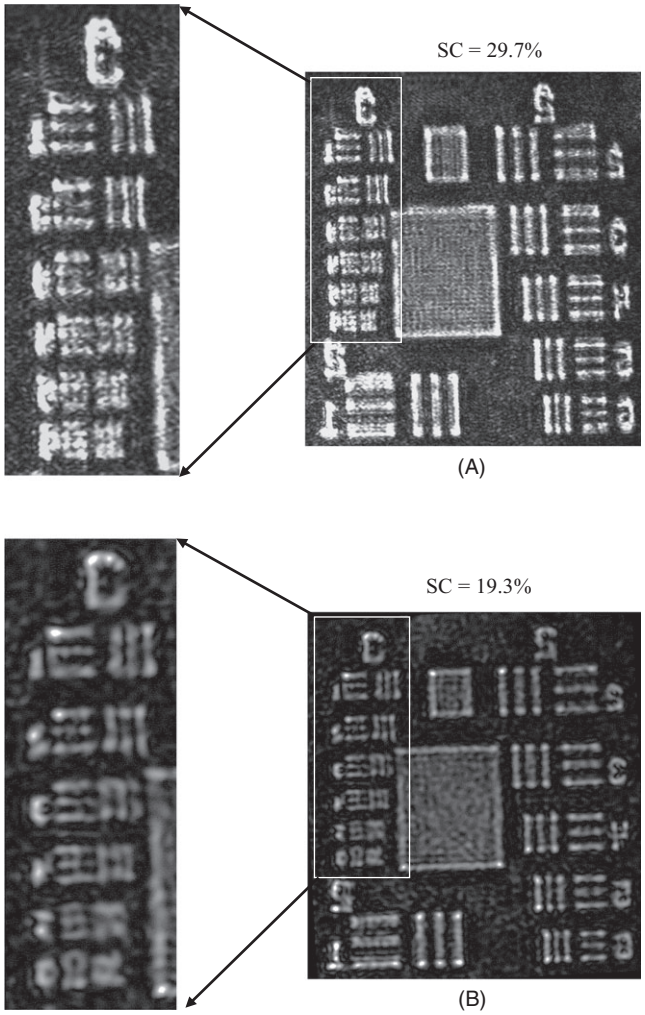

FIGURE 11 (A) is the captured image with an enlarged view given by the SSB on DMD 2, and (B) is the captured image with an enlarged view given by the programmed filter on DMD 2

mirrors with a large diameter equal to the spectrum spot size of the single carrier waves can be applied to solve this problem. In addition, a horizontal shrinkage is observed in the captured hologram images when the DMDs are used as a spatial filter. This is caused by the misalignment of DMD 2 although we tried to adjust it as possible as we can. Thus, the image is horizontally distorted. Although the refresh rate of the DMDs in the temporal multiplexing experiments was 3,600 Hz for convenience, it could be dynamically altered in other applications.

6 | SUMMARY AND CONCLUSION

Previously reported works gave a good description for reducing the speckle artifacts in binary-type holographic display systems. However, the conventional approaches did not provide delicate considerations in the filtering technique. Our proposed concept features how to effectively filter the unwanted signal spectra to recover hologram images with reduced speckle artifacts. In addition, to estimate the speckles, we designed a test image pattern and quantified them with speckle contrast values. Thus, it has been proved that our proposed programmable filter can effectively reduce speckle artifacts compared to the conventional filtering technique.

ORCID

Yongjun Lim https://orcid.org/0000-0003-3285-0651

REFERENCES

1. J. W. Goodman, *Speckle phenomena in optics: Theory and Applications*, Roberts and Company Publishers, Englewood, CO, USA, 2007.
2. J. Hong et al., *Three-dimensional display technologies of recent interest: Principles, status, and issues*, Appl. Opt. **50** (2011), no. 34, H87–H115.
3. L. Onural, F. Yaras, and H. Kang, *Digital holographic three-dimensional video display*, Proc. IEEE **99** (2011), no. 4, 576–589.
4. F. Yaraş, H. Kang, and L. Onural, *Real-time phase-only color holographic video display system using LED illumination*, Appl. Opt. **48** (2009), no. 34, H48–H53.
5. T. S. McKechnie, *Speckle reduction in laser speckle and related phenomena*, J. C. Dainty ed., Springer-Verlag, Berlin/Heidelberg, 1975.
6. V. Bianco et al., *Strategies for reducing speckle noise in digital holography*, Light Sci. Appl. **7** (2018), no. 1, 48:1–48:16.
7. V. Bianco et al., *Quasi noise-free digital holography*, Light Sci. Appl. **5** (2016), no. 9, e16142:1–e16142:12.
8. A. Uzan, Y. Rivenson, and A. Stern, *Speckle denoising in digital holography by nonlocal means filtering*, Appl. Opt. **52** (2013), A195–A200.
9. M. Leo et al., *Automatic digital hologram denoising by spatiotemporal analysis of pixel-wise statistics*, J. Display Technol. **9** (2013), no. 11, 904–909.
10. M. Leo et al., *Multilevel bidimensional empirical mode decomposition: A new speckle reduction method in digital holography*, Opt. Eng. **53** (2014), no. 11, 112314:1–112314:10.
11. P. Memmolo et al., *Encoding multiple holograms for speckle-noise reduction in optical display*, Opt. Express **22** (2014), no. 21, 25768–25775.
12. Y. Rivenson, A. Stern, and J. Rosen, *Compressive multiple view projection incoherent holography*, Opt. Express **19** (2011), no. 7, 6109–6118.
13. Y. Takaki and M. Yokouchi, *Speckle-free and grayscale hologram reconstruction using time-multiplexing technique*, Opt. Express **19** (2011), no. 8, 7567–7579.
14. T. Kurihara and Y. Takaki, *Speckle-free, shaded 3D images produced by computer-generated holography*, Opt. Express **21** (2013), no. 4, 4044–4054.
15. S. -B. Ko and J. -H. Park, *Speckle reduction using angular spectrum interleaving for triangular mesh-based computer-generated hologram*, Opt. Express **25** (2017), no. 24, 29788–29797.
16. T. M. Kreis, P. Aswendt, and R. Hoefling, *Hologram reconstruction using a digital micromirror device*, Opt. Eng. **40** (2001), no. 6, 926–933.
17. J. -Y. Son et al., *Holographic display based on a spatial DMD array*, Opt. Lett. **38** (2013), no. 16, 3173–3176.

18. T. Inoue and Y. Takaki, *Table screen 360-degree holographic display using circular viewing-zone scanning*, Opt. Express **23** (2015), no. 5, 6533–6542.
19. O. Bryngdahl and A. Lohmann, *Single-sideband holography*, J. Opt. Soc. Am. **58** (1968), no. 5, 620–624.
20. Y. Takaki and Y. Tanemoto, *Band-limited zone plates for single-sideband holography*, Appl. Opt. **48** (2009), no. 34, H64–H70.
21. J. -H. Park, *Recent progresses in computer generated holography for three-dimensional scene*, J. Inform. Display **18** (2017), no. 1, 1–12.
22. Y. Lim et al., *360-degree tabletop electronic holographic display*, Opt. Express **24** (2016), no. 22, 24999–25009.
23. M. Kim et al., *Expanded exit-pupil holographic head-mounted display with high-speed digital micromirror device*, ETRI J. **40** (2018), no. 5, 366–375.
24. C.-M. Chang and H.-P. D. Shieh, *Design of illumination and projection optics for projectors with single digital micromirror devices*, Appl. Opt. **39** (2000), no. 22, 3202–3208.
25. J.-W. Pan et al., *Portable digital micromirror device projector using a prism*, Appl. Opt. **46** (2007), no. 22, 5097–5102.
26. J. W. Goodman, *Some fundamental properties of speckle*, J. Opt. Soc. Am. **66** (1976), no. 11, 1145–1150.
27. D.A. Boas and A. K. Dunn, *Laser Speckle Contrast Imaging in Biomedical Optics*, J. Biomed. Opt. **15** (2010), no. 1, 011109:1–011109:12.

AUTHOR BIOGRAPHIES

Yongjun Lim received his PhD degree from Seoul National University, Korea in 2010. From 2011 to 2014, he worked for Samsung Electronics as a senior engineer. Since 2014, he has been working for ETRI, Daejeon, Rep. of Korea where he is now a senior researcher. His research interests include electronic holographic display systems, holographic microscopy, optical lithography, non-diffracting beams, surface plasmons, diffractive optics and near-field optics.

Jae-Hyeung Park received his BS, MS, and PhD degrees from Seoul National University, Korea in 2000, 2002, and 2005, respectively. From 2005 to 2007, he worked for Samsung Electronics as a senior engineer. In 2007, he joined the faculty member of Chungbuk National University, Korea. Since 2013, he has been with Inha University where he is now a full professor of the department of information and communication engineering. His research interests include light field and holographic information processing and display techniques.

Joonku Hahn received his PhD degree in 2009 from School of Electrical Engineering, Seoul National University, Seoul, Korea. In 2011, he joined the faculty of school of electronics engineering, Kyungpook National University, Daegu, Rep. of Korea, and he is now an associate professor. His main interests are 3D display and digital holography applications.

Hayan Kim received her BS and MS degrees in optical engineering from the School of Electronics and Information Engineering, Sejong University, Seoul, Rep. of Korea, in 2014 and 2016. Since 2016, she has been with the Electronics and Telecommunications Research Institute, Daejeon, Rep. of Korea, where she is now a researcher. Her main research interests include digital holography and holographic display system.

Keehoon Hong received his BS degree in Electrical and Electronic Engineering from Yonsei University, Seoul, Korea in 2008 and his PhD degree in Electrical Engineering and Computer Science from Seoul National University, Seoul, Korea in 2014. He is currently working as a Senior Researcher for Electronics and Telecommunications Research Institute, Daejeon, Rep. of Korea. His research interests include autostereoscopic display, digital holographic display, and holographic optical elements.

Jinwoong Kim received his BS and MS degrees in electronics engineering from Seoul National University, Seoul, Rep. of Korea, in 1981 and 1983, respectively. He received his Ph.D. degree in electrical engineering from Texas A&M University, College Station, TX, USA, in 1993. He has been working for ETRI, Daejeon, Rep. of Korea since 1983, leading many projects in the telecommunications and digital broadcasting areas.